Large-scale self-assembly of dispersed nanodiamonds

Houjin Huang,[a] Liming Dai,*[a] David H. Wang,[b] Loon-Seng Tan[c] and Eiji Osawa[d]

Received 29th October 2007, Accepted 8th January 2008
First published as an Advance Article on the web 31st January 2008
DOI: 10.1039/b716676a

Well-aligned rectangular-shaped nanodiamond fibers (NDFs) with a length-to-width ratio of over 1000 were formed on a large-scale *via* a self-assembly process by drying acid-treated nanodiamonds of a uniform size (~4 nm) from an aqueous solution. Nanodiamond thin films (NDTFs), instead of NDFs, have also been prepared by drying the aqueous ND dispersion at a sufficiently low temperature (< 70 °C)) and/or a sufficiently low pH (< 4). Detailed conditions, including pH and temperature, for the formation of NDFs and NDTFs *via* the drying process, together with the structure and property of the resultant nanodiamond assemblies were investigated. The formation of NDFs and NDTFs was found to result from the delicate interplay between the ND–ND, ND–H_2O, and ND–substrate interactions under the water-evaporation-induced directional convection flow. The resultant NDFs were demonstrated to show a bandgap of ~4.5 eV.

Introduction

Carbon has long been known to exist in three forms: amorphous carbon, graphite and diamond.[1] Depending on how the carbon atoms are arranged, their properties vary. Graphite is soft and black due to the layered arrangement of carbon hexagons, whereas diamond is hard and transparent because of the regular repetitive pattern of fully bonded carbon atoms in 3-dimensional space. The discovery of buckminsterfullerene C_{60} in 1985 by Kroto *et al.*[2] created an entirely new branch of carbon chemistry.[1] The subsequent discovery of carbon nanotubes in 1991 by Iijima[3] opened up a new era in materials science and nanotechnology.[1] Since then, carbon nanotechnology has become one of the major building blocks for the entire field of nanotechnology. With the rapid development of nanotechnology, nanodiamonds have attracted a great deal of attention as a recent addition to the nanocarbon family.[4]

Having the diamond structure on a nanometre scale, nanodiamonds exhibit exceptional hardness, fracture strength, environmental inertness, and optoelectronic properties attractive for a variety of important applications, including field-emission displays, nanotribology, miniaturized mechanical and optoelectronic systems, and biomedical nanodevices.[1,4,5] For these, and many other, applications, it is highly desirable to have nanodiamonds prepared in a thin fiber-like and/or film form. However, it has been impossible to form the pure diamond-like fiber or film from any preformed nanodiamonds due to their super-hard and inert nature, though the formation of thin coatings of chemically-functionalized/polymer-grafted nanodiamonds has been demonstrated recently.[6] As a consequence, chemical vapor deposition (CVD) remains a major technology for the formation of pure diamond thin films. However, the expensive set-up and substrate-specific nature associated with the CVD process have severely limited many potential applications (*e.g.* flexible devices).[7]

The readily available detonation nanodiamonds[4a] and the recent breakthrough in disintegrating them into stable aqueous colloidal solution of nanodiamond particles having diameters of 4–5 nm provide new fundamental and applied opportunities. In this paper, we report our recent work on purification of the detonation nanodiamonds through acid treatment and their large-scale self-assemby into one-dimensional nanodiamond fibers (NDFs) with a length-to-width ratio of over 1000 and two-dimensional nanodiamond thin films (NDTFs). Electrical property measurements on the resultant NDFs revealed their wide bandgap nature (~4.5 eV) attractive for many potential applications in various microelectronic and optoelectronic devices.[8–14]

Experimental

Nanodiamond (ND) samples in the form of black crystalline-like powder consisting of ~4 nm primary particles were supplied by NanoCarbon Research Institute Ltd in Japan. These samples were originally prepared by detonation of explosives in an inert atmosphere,[15] and then subjected to disintegration by stirred media milling.[4a]

For purification, the *as-received* nanodiamond sample was first treated with an aqueous acid mixture (70% HNO_3 and 98% H_2SO_4 in a ratio of 1 : 3) in a sonication bath (model 75D, VWR) for 1 hour, followed by reflux at 180 °C for three days. Excess acid was then removed by repeatedly centrifuging (10 000 g) and decanting. The precipitate recovered from centrifugation was then dispersed in water at pH > 4.0. The concentration of the resultant aqueous dispersion of nanodiamonds was determined by simply drying a certain volume of the dispersion and measuring the dry weight. NDFs or NDTFs were formed on glass substrates by drying an aqueous dispersion of nanodiamonds under appropriate conditions, as described in the

[a]*Department of Chemical and Materials Engineering, University of Dayton, 300 College Park, Dayton, OH 45469, USA. E-mail: ldai@udayton.edu*
[b]*University of Dayton Research Institute, 300 College Park Avenue, Dayton, OH 45469-0060, USA*
[c]*Nanostructured & Biological Materials Branch, Materials and Manufacturing Directorate, Air Force Research Laboratory, AFRL/RXBP & RXBP/UDRI, Wright-Patterson AFB, OH 45433, USA*
[d]*NanoCarbon Research Institute, Ltd, Chiba, Kashiwa, Japan*

text below. Prior to its use for the self-assembly, the glass substrate (*i.e.* microscope plate from VWR) was first cleaned with ethanol (99.5%) followed by air flow drying, leading to a sessile air–water contact angle of less than 15°. The pH value was measured using a pH meter (Hanna instruments, model pH212). The chemical nature of the nanodiamonds before and after the acid treatment was characterized using Raman spectroscopy (514.5 nm laser, Renishaw, inVia reflex microRaman), Fourier transform infrared spectroscopy (FTIR, Perkin-Elmer Spectrum ONE), UV/visible spectroscopy (UV-Vis, Perkin-Elmer Lambda 900), thermal gravimetric analysis (TGA, TA instruments), and X-ray photoelectron spectroscopy (XPS, SSX-100), while their morphological structures were examined on a scanning electron microscope (SEM, Hitachi S-4800 HRSEM) and transmission electron microscope (TEM, Hitachi H-7600). Electrical properties of the NDFs and NDTFs were measured with a precision semiconductor analyzer (Agilent 4156C).

Results and discussion

Acid treatment of nanodiamonds

The acid treatment has been previously used for purification of detonation nanodiamonds.[16] Fig. 1 gives a photo showing aqueous dispersions of the acid-purified (Fig. 1a) and *as-received* (Fig. 1b) nanodiamonds. It can be seen that the acid treatments greatly reduced the black color for the *as-received* nanodiamonds dispersed in water.

Fig. 2a reproduces the TGA curves, which show a major decomposition temperature of ~570 °C for both the acid-purified NDs (designated as ND–COOH, *vide infra*) and the *as-received* NDs (designated as DN-raw or Raw-DNs). The insets of Fig. 2a show some noticeable differences between the acid-purified and *as-received* ND samples. There are oxidation-induced weight gains of about 0.5 and 2.2% at ~447 °C for the acid-purified and *as-received* diamond samples, respectively. Besides, the temperatures corresponding to the completed weight loss are about 679 °C for the acid-purified NDs and 649 °C for the *as-received* diamond sample. Because sp^2 carbons can not only cause a weight gain by thermally oxidizing them into various oxygen-containing groups (*e.g.* –COOH) but also a reduced burning-off temperature for diamonds through co-burning the diamonds with the sp^2 carbons, the above observed differences in the thermal gravimetric data indicate that the acid treatment has effectively removed the sp^2 carbons in the diamond sample. Assuming the observed weight gain is due to the conversion of sp^2 carbons into –COOHs, we can estimate that the amount of sp^2 carbons in the acid-purified NDs is ~0.18 %wt, which is ~4.5 times lower than that in the *as-received* diamond sample (~0.8 %wt). The richness of sp^2 carbons in the *as-received* diamond sample is also evidenced by its much stronger optical absorption at the low wavelength region both in the solid film (Fig. 2b) and an aqueous dispersion (inset of Fig. 2b). The cut-off optical absorption extended from ~600 to ~1200 nm (near IR region) for the *as-received* diamond sample upon drying up from the aqueous dispersion, a much more pronounced red-shift than the acid-purified NDs. While the strong low-wavelength absorption can be assigned to the presence of conjugated sp^2 carbons, the observed red-shift upon drying is attributable to possible extension of the π-conjugation through interparticle contacts of the sp^2 carbons.

The effectiveness of the acid treatment to remove sp^2 carbons can be clearly seen in Fig. 2c, which shows Raman spectra of the

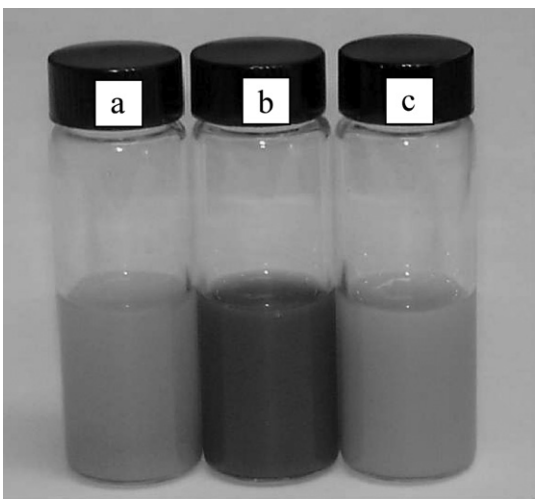

Fig. 1 Photo showing aqueous dispersions of (a) acid-purified, (b) as-received, and (c) base-purified nanodiamond samples (*vide infra*). The concentrations of the dispersions are ~0.4 %wt.

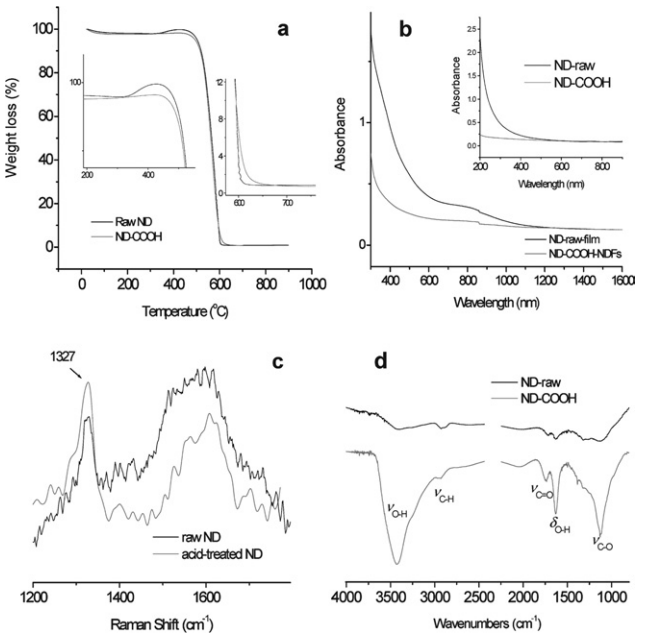

Fig. 2 Characterization of the *as-received* and acid-purified ND samples: (a) TGA of the raw NDs (black) and acid-purified NDs (grey). The insets show two portions just before and after the major weight loss. The heating rate is 5 °C min^{-1}. (b) UV-Vis of the ND solid before and after the acid purification. The inset shows UV-Vis of the NDs before and after the acid purification in an aqueous dispersion. The spectra are normalized to the same concentration. (c) Raman spectra of the NDs before (grey) and after (black) the acid purification. The excitation wavelength of the laser is 514.5 nm. (d) FTIR spectra of the NDs before and after the acid purification in the film form. The adsorbed water in NDs was removed by heating the sample in air for 150 °C for one hour prior to the FTIR measurements.

diamond sample before and after the acid purification. Compared to the *as-received* diamond sample, the acid-purified NDs showed a much higher peak area ratio of sp^3 (~1327 cm^{-1}) to sp^2 (1450–1700 cm^{-1}, G-band), which increased from ~0.10 for the former to ~0.50 for the later.[14] Although Raman spectra of nanodiamonds depend also on the primary particle size,[14] this ~5 times enhancement in the peak area ratio of sp^3 to sp^2 presumably indicates a significant removal of sp^2 carbons by the acid-purification, consistent with the TGA data (*vide supra*).

As noted by Osawa *et al.*,[4a] it is difficult to isolate detonation nanodiamonds in the pure form. Similar to the formation of fullerols,[17] fullerene-like surface of nanodiamonds (as evidenced in dark-brown color of the *as-received* NDs)[18a] can be oxidized by the strong acid to form "nanodiamondols" (NDols) with many –OH and –COOH functional surface groups, as confirmed by the much higher relative FTIR peak ratios of those O-containing peaks to the C–H peak seen in Fig. 2d for the acid-purified ND with respect to the *as-received* ND. Our preliminary results indicate that strong base (NaOH, pH~14) treatments in a sonication bath (model 75D, VWR) can also lead to nearly pure and water-dispersible nanodiamonds (see, Fig. 1c). More detailed discussions on the Raman and FTIR spectra of diamond powders have been reported previously,[14b,18b,c] which would be beyond the scope of this manuscript focusing on communicating the new self-assembling properties of the modified nanodiamonds.

Formation of NDFs and NDTFs

A TEM image for the acid-purified NDs is given in Fig. 3a, which revealed a particle size distribution in the range of 2–6 nm with an average value of ~4 nm. As shown in Fig. 3b, NDFs with a rectangular cross-section and a length of over 2 cm can easily be obtained by drying an aqueous dispersion (pH ≥ 4.4) of the acid-treated nanodiamonds on a glass hotplate at ~85 °C. It was noted that the drying process started from the drop rim and gradually moved towards the center to form radially aligned NDFs. Cracks with sharp edges were seen once the ND film was dried. The length of the resultant NDFs is limited only by the drop size; NDFs with a length over 5 cm have been obtained. The width of the NDFs after cracking is typically in the range of 10~100 μm (*cf.* Fig. 6a). More interestingly, a semitransparent ND thin film (NDTF, Fig. 3c), instead of NDFs, was formed when an aqueous dispersion of the acid-treated nanodiamonds with pH ≈1.0 was dried up at room temperature. In contrast, we observed neither well-structured NDF nor NDTF when the *as-received* diamond sample dispersed in water was used as the starting material. Although the similar FTIR peaks seen in Fig. 2d for both the acid-purified and *as-received* NDs could indicate that the *as-received* ND might have been subjected to the similar acid purification by manufacturer, the number of those oxygen-containing groups introduced by the original acid treatment is obviously insufficient to support the self-assembly process.

The formation of NDFs or NDTFs from aqueous dispersions of the acid-treated NDs is affected by various factors, including pH, temperature, and concentration. As can be seen in Fig. 4a, no NDFs, but NDTFs only, could be produced when the pH value was below 4.0 even with other factors being optimized

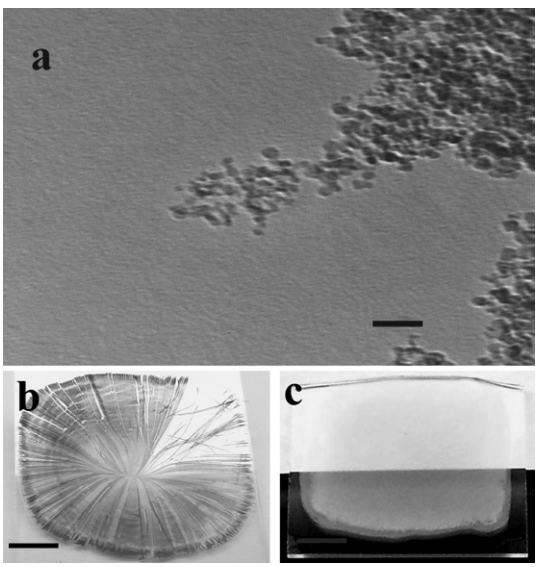

Fig. 3 (a) A TEM image showing the acid-treated NDs with particle sizes in the range of 2~6 nm. The scale bar represents 20 nm. (b) NDFs formed from its aqueous dispersion with a pH value of 4.8 on a glass substrate heated at 85 °C. (c) NDTF formed from the ND dispersion with a pH value of 1.0 on a glass substrate at room temperature (20 °C); its semi-transparency is illustrated by the visibility of the dark substrate beneath the NDTF at the bottom half. The scale bars in (b) and (c) represent 1 cm.

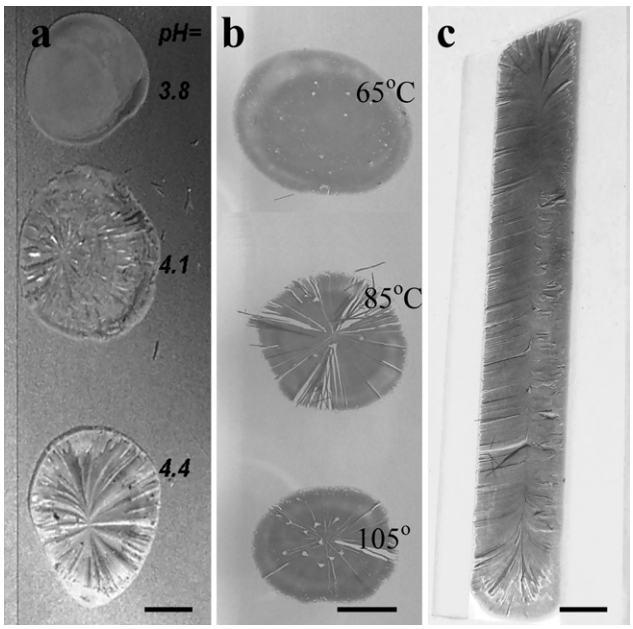

Fig. 4 Photos showing the formation of various NDFs and NDTFs under different conditions: (a) and (b) show the effects of pH and temperature on the formation of NDFs, respectively. The substrate temperature is 85 °C for (a). The pH value of the ND dispersion is 4.8 for (b). (c) Aligned NDFs formed from an aqueous solution of the acid-treated NDs within a confined channel formed by two parallel Scotch-tapes on a glass plate. The substrate temperature for (c) is the same as that for (a) and the pH value of the ND dispersion for (c) is the same as that for (b). The concentrations of the ND dispersions for (a)~(c) are the same (*i.e.* 30 mg ml^{-1}). All the scale bars represents 1 cm.

(85 °C, 30 mg ml^{-1}). With some fragmented ND flakes becoming observable at pH ≈ 4.1, further increase in pH up to 4.4 led to the formation of well-structured NDFs. The optimum pH for the formation of NDFs was found to be between 4.4 and 5.5 – the higher pH in this range, the easier the formation of NDFs. Due to the presence of acidic functional groups on NDs, however, the highest achievable pH value for the ND dispersion is ~5.5. Apart from the pH value, temperature also played an important role in the self-assembly process.

As shown in Fig. 4b, NDFs could easily be prepared when the substrate was heated at about 85 °C, but no well-structured NDF was formed when the substrate temperature was either below ~70 °C or above ~100 °C even with other factors being optimized (pH ≈ 4.8, 30 mg ml^{-1}). Furthermore, we found that the formation of NDFs or NDTFs depended also on the ND concentration with NDFs being more easily obtained for highly concentrated ND dispersions (> *ca.* 10 mg ml^{-1}). At a lower concentration, no NDF was observed.

Formation mechanism of NDFs and NDTFs

To understand the formation mechanism for the NDFs or NDTFs, we need to consider both the water-convection flow and interactions of the acid-purified NDs with the liquid medium and substrate during the drying process. In view of a recent publication on the water-freezing-induced construction of lamellar microstructures,[19] we proposed a relevant NDF-formation mechanism, as schematically shown in Fig. 5. Similar to the published work in which the growing ice crystals repel ceramic nanoparticles,[19] we believe that the water-evaporation-induced convection, coupled with the particle–particle, particle–water, and particle–substrate interactions (*vide infra*), is the driving force for the formation of NDFs in our system. The water-evaporation-induced convection in our case was caused by the temperature difference between the rim region and center of the ND dispersion droplet. Typically, a temperature difference of about 4 °C was found between the rim and center for a ND dispersion droplet of 2 cm on a glass plate heated up to about 85 °C by a hot-plate. Due to the presence of the temperature gradient, the water-evaporation-induced convection flow can be controlled to proceed along certain directions under appropriate conditions, as exemplified by Fig. 3b and Fig. 4c (*vide supra*). However, the actual situation can be much more complicated. Various interactions, including ND–water, ND–ND, ND–substrate, could also regulate the formation of NDFs or NDTFs. Due to the presence of –OH/–COOH surface groups on the acid-treated NDs, hydrogen bonding is believed to be the major interaction among ND–H_2O and ND–ND. Besides, the π–π interaction associated with the remaining sp^2 carbons on the acid-treated NDs and the van der Waals force cannot be excluded from the ND–ND interaction. The ND–substrate interaction is mainly due to the weak van der Waals attraction, along with a certain extent of hydrophilic–hydrophilic interaction. The formation of NDFs or NDTFs is believed to result from the delicate balance of these interactions under the directional water convection. NDFs could form under an appropriate water-convection flow when ND–ND > ND–H_2O > ND–substrate, whereas NDTFs only might be produced if ND–ND or ND–substrate became stronger than ND–H_2O and under a relatively weak water-convection flow.

Although it is still somewhat superficial, the above proposed mechanism enabled us to understand many of the observations mentioned earlier. As shown in Fig. 4b, for example, NDFs can form only within a certain temperature range as water convection may be either insufficiently strong at a low temperature (< 70 °C) or too chaotic at a high temperature (> 95 °C). Also, a low pH (< 4.0) may favor the sedimentation of the acid-treated NDs out from the aqueous dispersion, due to the reduced surface-charge repulsion *via* protonation of oxygenated surface groups (*e.g.* COO^-), which could minimize the directional effect by the water convection to form the NDTF (Fig. 4a). These understandings prompted us to use a confined self-assembly method for preparing NDFs with a well-defined structure and orientation, as described below.

Controlled formation of NDFs

The orientation of NDFs can be controlled by self-assembly of the acid-treated NDs from an aqueous dispersion within a confined space. As shown in Fig. 4c, well-aligned NDFs were produced within a confined channel formed by two parallel Scotch tapes. In this case, the drying process of the acid-treated NDs started from the inner edge of both Scotch tapes and gradually proceeded towards the central line in the middle of the channel

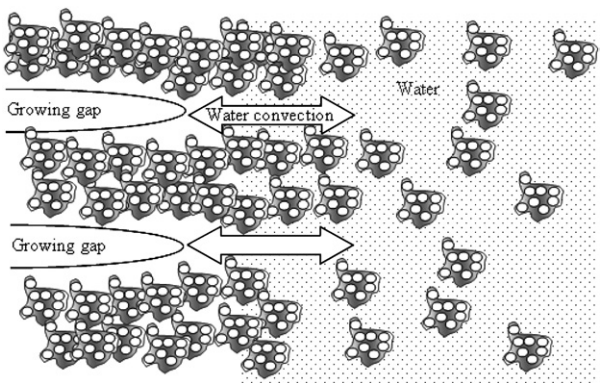

Fig. 5 Schematic model showing the formation process of NDFs. Double arrows indicate the directions of water flow induced by evaporation (to the left) and shrinking of the ND aqueous drop (to the right).

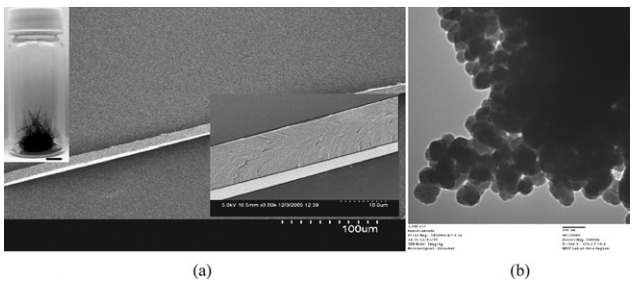

Fig. 6 (a) A SEM image of a typical NDF. The right side inset shows an enlarged view of the NDF while the left side inset is a photo image showing NDF samples in a bottle. The scale bar in the left side inset represents 1 cm. (b) A typical edge-view TEM image of the NDF (scale bar represents 100 nm).

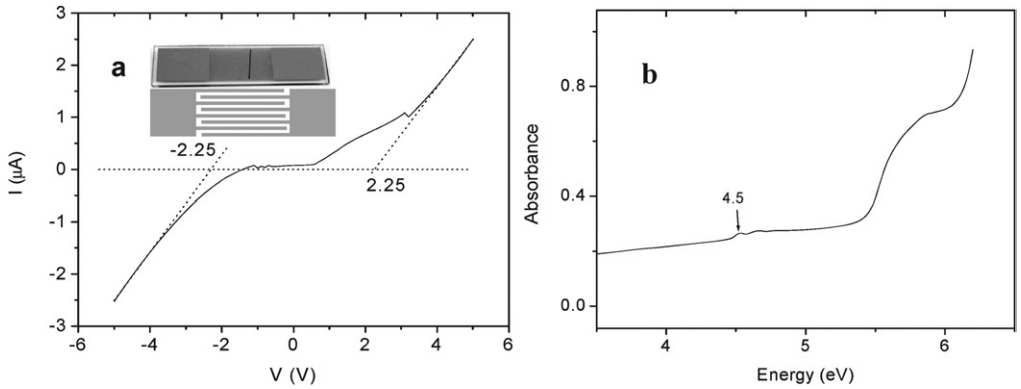

Fig. 7 (a) *I–V* curve of an individual NDF and (b) optical absorption of highly dispersed NDs. The NDF was annealed at 800 °C in vacuum for 3 min. The insets in (a) show a photo image (top) and a schematic drawing (bottom) of a single NDF on interdigited Au electrodes with a 50-μm gap for the *I–V* measurements. The contact of the NDF and the Au electrodes was improved by slightly wetting the NDF with anhydrous ethanol and quickly drying on a hot plate at 200 °C. The highly dispersed NDs were obtained by centrifuging to remove the ND aggregates at 2000 rmp for 1 hour, followed by sonication for 1 hour. The pH for the ND dispersion is ~5.5.

along the direction normal to the tape length. Interestingly, it is noticed that the NDFs formed on both sides of the central line within the channel are different in their length and orientation perfection. The longer NDFs formed at the left half of Fig. 4c appeared to have a better parallel orientation perfection, indicating that a higher drying speed could lead to a better alignment in this particular case.

Structure and property of NDFs

Fig. 6a shows a typical SEM image of NDFs. It can be seen that the cross-section of the NDF takes a rectangular shape with rather sharp edges. The width and thickness for this particular NDF are about 11 and 2 μm, respectively; and its length is over 2 cm (see, the NDF sample in the left side inset of Fig. 6a) so that the length-to-width ratio reaches over 1000. Surprisingly, the resultant NDF has very smooth surfaces and a uniform thickness along its long axis, indicating no pill-up agglomeration of NDs along the drying direction. A typical edge-view TEM image of NDFs is given in Fig. 6b, which shows agglomerates with a grain size over 20–50 nm. We may speculate that acid-treated nanodiamond primary/secondary particles agglomerated through van der Waals/hydrophilic–hydrophilic interactions during the self-assembly process.[14b] Although the NDFs are bound mainly through non-covalent interactions, including hydrogen bonding, π–π interactions, and van der Waals forces, they can be produced in a free-standing form (inset of Fig. 6a) with appropriate mechanical properties for subsequent measurements of their electronic properties to be described below.

We have also measured *I–V* curves for individual NDFs after annealing at 800 °C in vacuum. Although there is a possibility that prolonged heat treating (several hours) of the diamond in vacuum at high temperature (≥ 900 °C) may cause back transformation of diamond to graphic,[20] no such back transformation, but merely removal of residual ethanol/water, was observed by heating the NDF sample at 800 °C for only a couple of minutes. A distinct bandgap structure has been observed for the NDFs, as shown in Fig. 7a from which the bandgap value of *ca.* 4.5 eV was obtained by extrapolating both of the nearly linear regions of the *I–V* curves at each of the high voltage sides to zero current.

The bandgap structure deduced from the *I–V* curve for the NDF is consistent with the optical absorption of the highly dispersed acid purified NDs (Fig. 7b), which shows an absorption band around 4.5 eV. This distinct *I–V* curve and optical absorption feature were unobservable in the *as-received* diamond sample, indicating the importance of the purification process for revealing the bandgap structure of NDs. A small amount of sp^2 carbons remained even after rigorous purification. As seen in Fig. 7a, the residual sp^2 carbons induced the non-zero current within the bandgap. These NDFs with unique electrical properties may be useful for various applications, ranging from their potential use in microelectronic devices, through optical waveguide systems, to multifunctional composites.[8–14]

Conclusions

We have demonstrated for the first time the large-scale formation of macroscopic NDFs and semitransparent NDTFs using detonation nanodiamonds after acid purification. The NDF/NDTF formation mechanism and conditions have been investigated. As a result, we proposed a water-evaporation-induced convection model to explain the self-assembly of the acid-treated NDs into NDFs and NDTFs. By self-assembly within a confined space, the orientation of the resultant NDFs can be effectively controlled. Our *I–V* measurements on individual NDFs revealed a distinct bandgap of 4.5 eV, correlating well with their optical absorption. Due to the simplicity and versatility characteristic of the acid-purification and subsequent self-assembly, the methodology developed in this study could be regarded as a general approach toward the production of large-scale diamond materials with controlled structures and properties for various potential applications.

Acknowledgements

LD and EO thank NEDO (04IT4) for financial support. LST is thankful for the support from AFOSR and AFRL/ML.

References

1 L. Dai, *Carbon Nanotechnology: Recent Developments in Chemistry, Physics, Materials Science and Device Applications*, Elsevier, Amsterdam, 2006.
2 H. W. Kroto, J. R. Health, S. C. O'Brien, R. F. Curl and R. E. Smalley, *Nature*, 1985, **318**, 162.
3 S. Iijima, *Nature*, 1991, **56**, 354.
4 (*a*) See, for example: A. Kruger, F. Kataoka, M. Ozawa, T. Fujino, Y. Suzuki, A. Aleksenskii, A. Vul' and E. Osawa, *Carbon*, 2005, **43**, 1722, and references cited therein; (*b*) V. V. Danilenko, *Phys. Solid State*, 2004, **46**, 595; (*c*) O. A. Williams, *Semicond. Sci. Technol.*, 2006, **21**, R49; (*d*) T. S. Huang, Y. Tzeng, Y. K. Liu, Y. K. Chen, K. R. Walker, R. Guntupalli and C. Liu, *Diamond Relat. Mater.*, 2004, **13**, 1098; (*e*) V. I. Kurmashev, Y. V. Timoshkov, T. I. Orehovskaja and V. Y. Timoshkov, *Phys. Solid State*, 2004, **46**, 696; (*f*) M. Ozawa, M. Inaguma, M. Takahashi, F. Kataoka, A. Kruger and E. Osawa, *Adv. Mater.*, 2007, **19**, 1201; (*g*) C. C. Fu, H. Y. Lee, K. Chen, T. S. Lim, H. Y. Wu, P. K. Lin, P. K. Wei, P. H. Tsao, H. C. Chang and W. Fann, *Proc. Natl. Acad. Sci. U. S. A.*, 2007, **104**, 727.
5 A. M. Schrand, H. Huang, C. Carlson, J. J. Schlager, E. Osawa, S. M. Hussain and L. Dai, *J. Phys. Chem. B*, 2007, **111**, 2, and references cited therein.
6 (*a*) See, for example: L. Li, J. L. Davidson and C. M. Lukehart, *Carbon*, 2006, **44**, 2308; (*b*) H. Sawada, J. Kurachi, H. Takahashi, K. Ueno and K. Hamazaki, *Polym. Adv. Technol.*, 2005, **16**, 651; (*c*) Y. Liu, V. N. Khabashesku and N. J. Halas, *J. Am. Chem. Soc.*, 2005, **127**, 3712; (*d*) Y. Liu, Z. N. Gu, J. L. Margrave and V. N. Khabashesku, *Chem. Mater.*, 2004, **16**, 3924.
7 D. M. Gruen, *Annu. Rev. Mater. Sci.*, 1999, **29**, 211.
8 R. J. Trew, J. B. Yan and P M. Mock, *Proc. IEEE*, 1991, **79**, 598.
9 M. Prato, *Top. Curr. Chem.*, 1999, **199**, 173.
10 P. Poulin, B. Vigolo and P. Launois, *Carbon*, 2002, **40**, 1741.
11 W. Gebhardt, *Mater. Sci. Eng., B*, 1992, **11**, 1.
12 W. B. Chio, J. J. Cuomo, V. V. Zhirnov, A. F. Myers and J. J. Hren, *Appl. Phys. Lett.*, 1996, **68**, 720.
13 V. N. Khabashesku, J. L. Margrave and E. V. Barrera, *Diamond Relat. Mater.*, 2005, **14**, 859.
14 (*a*) S. Osswald, G. Yushin, V. Mochalin, S. O. Kucheyev and Y. Gogotsi, *J. Am. Chem. Soc.*, 2006, **128**, 11635; (*b*) G. N. Yushin, S. Osswald, V. I. Padalko, G. P. Bogatyreva and Y. Gogotsi, *Diamond Relat. Mater.*, 2005, **14**, 1721.
15 N. R. Greiner, D. S. Phillips, J. D. Johnson and F. Volk, *Nature*, 1988, **333**, 440.
16 (*a*) A. I. Shames, A. M. Panich, W. Kempinski, A. E. Alexenskii, M. V. Baidakova, A. T. Dideikin, V. Y. Osipov, V. I. Siklitski, E. Osawa, M. Osawa and A. Yul', *J. Phys. Chem. Solids*, 2001, **63**, 1993; (*b*) T. Fujimura, M. Sone, V. Y. Dolmatov and S. Shiozaki, *US Pat.*, 7115325.
17 L. Y. Chiang, R. B. Upasani, J. W. Swirczewski and S. Soled, *J. Am. Chem. Soc.*, 1993, **115**, 5453.
18 (*a*) J. Y. Raty, G. Galli, C. Bostedt, T. W. van Buuren and L. J. Terminello, *Phys. Rev. Lett.*, 2003, 90, 037401; (*b*) T. Jiang and K. Xu, *Carbon*, 1995, **33**, 1663; (*c*) T. Jiang, K. Xu and S. Ji, *J. Chem. Soc., Faraday Trans.*, 1996, **92**, 3401.
19 S. Deville, E. Saiz, R. K. Nalla and A. P. Tomsia, *Science*, 2006, **311**, 515.
20 B. L. V. Prasad, H. Sato, T. Enoki, Y. Hishihiro, Y. Kaburagi, A. M. Rao, P. C. Eklund, K. Oshida and M. Endo, *Phys. Rev. B: Condens. Matter*, 2000, **62**, 11209.

